INSTITUTE OF PHYSICS PUBLISHING MEASUREMENT SCIENCE AND TECHNOLOGY

Meas. Sci. Technol. **16** (2005) 1730–1740 doi:10.1088/0957-0233/16/9/004

Electrical conductivity channel for a shock tube

Frank K Lu[1], **Hsuan-Cheng Liu**[2] **and Donald R Wilson**[1]

[1] Aerodynamics Research Center, Mechanical and Aerospace Engineering Department, University of Texas at Arlington, Arlington, TX 76019-0018, USA
[2] Aerospace Science and Technology Research Center, National Cheng Kung University, 198 Hsin-Sheng Street, Kuei-Jen, Tainan 711, Taiwan

E-mail: lu@mae.uta.edu, jonathan@astrc.iaalab.ncku.edu.tw and wilson@mae.uta.edu

Received 10 January 2005, in final form 7 June 2005
Published 25 July 2005
Online at stacks.iop.org/MST/16/1730

Abstract
The design of an electrical conductivity measurement channel for a shock tube is described. This measurement channel is used for the study of weakly ionized, high-enthalpy flows of gases seeded with alkali salts. The theory for determining the dimensions of the measurement channel and the electrical power supply for the channel is based on Ohm's law. Data are shown which demonstrate that the channel performs well. However, the measured electrical conductivity was one or two orders less than theoretical values. The current traces for each case show that the peak current occurred behind the contact surface, which indicates that some of the seed was entrained behind the test gas originally in the driven tube. An analysis of the effect of Joule heating on the measured conductivity was conducted. The result of increased temperature due to Joule heating in the measurement channel is believed to be minimal. Reasons for the discrepancy are given.

Keywords: ionized gas, plasma, shock tube

(Some figures in this article are in colour only in the electronic version)

Nomenclature

B	magnetic field
e	electron charge
E	electric field
I	current
J	current density
k	Boltzmann constant
MHD	magnetohydrodynamic
T	temperature
V	voltage
σ	conductivity
Subscripts	
add	additional
ei	electron–ion
en	electron–neutral

1. Introduction

Interest in magnetohydrodynamic (MHD) accelerators and decelerators [1, 2], hypersonic flow control [3], power extraction from hypersonic flows [4, 5] and hypersonic ground test facilities capable of true altitude simulation [6] has emphasized the need for a better understanding of the conductivity of the high-enthalpy, high-pressure gas involved. For example, the MHD accelerator utilizes the Lorentz $\mathbf{J} \times \mathbf{B}$ body force to increase the fluid velocity, pressure and temperature. The electrical conductivity of the operating fluid therefore plays an important role in determining the effectiveness of the accelerator. This requires that an MHD accelerator is provided with an electric field $\mathbf{E}$ at a reasonable electrode voltage range and an appropriate magnetic field $\mathbf{B}$. To ensure an adequate current, the gas flow must be electrically conductive. This may be realized in a neutral gas such as air by a preionization scheme or by seeding with a material which possesses a low ionization potential, for example, caesium or potassium salts.

The performance of MHD techniques with high-enthalpy gas flows depends directly on the magnitude of the electrical conductivity of the preionized or seeded gas. However, data on electrical conductivity of gaseous species are scarce or nonexistent at high pressures. For this reason, an electrical

conductivity channel was designed and fabricated for use with a high-performance shock tube. Electrical conductivity data were obtained for air and detonation products seeded with trace amounts of potassium or caesium carbonate. The data demonstrated proper performance of the channel.

2. Literature survey

Lin *et al* [7] proposed calculating the electrical conductivity of partially ionized gases by adding reciprocal conductivities of the form

$$1/\sigma_{\text{add}} = 1/\sigma_{\text{en}} + 1/\sigma_{\text{ei}}. \tag{1}$$

where σ_{en} is due to electron–neutral collisions and σ_{ei} is due to electron–ion collisions. Spritzer and Harm [8] proposed expressing the electron–ion conductivity by

$$\sigma_{\text{ei}} = 1.913 \times 10^4 \frac{(kT/e)^{3/2}}{\ln \Lambda} \quad \mho\,\text{m}^{-1}. \tag{2}$$

The quantity kT/e is the gas temperature expressed in electron volts while Λ is a parameter equal to the ratio of the Debye shielding distance to the impact parameter for 90° scattering by an ion. The conductivity due to electron–neutral collisions σ_{en} can be calculated as a function of the electron density from the Saha equation [9]. However, the conductivity calculated by this method is believed to be overestimated by 70% under some circumstances [10]. Garrison [10] proposed a modification to the Allis–Frost model [11, 12] that he referred to as a 'collision-mixing' model and showed that the results were in good agreement with the Demetriades–Argyropoulos model [13]. Furthermore, reasonable agreement between both models and his experimental results was achieved for pressures in the 0.1–5 atm range.

Much of the early experimental research obtained values of electrical conductivity that agreed with theoretical predictions [7, 14]. However, these experiments were performed at extremely low pressure, which is not appropriate for understanding the electrical conductivity of air at high-speed, air-breathing flight conditions [2]. It is only lately that efforts have been made to understand the electrical conductivity of gases at pressures relevant to air-breathing flight [4].

One of the early works at pressures of interest for air-breathing flight is that of Garrison [10]. His experiments involved nitrogen gas seeded with 1% molar fraction of potassium carbonate powder at a temperature range of 3000–4000 K and at a pressure of 0.65 atm. The experiments were conducted using a 2 MW arc heater. Seed material was injected into the mixing chamber located at the exit of the arc heater. The flow was then expanded to a Mach number of approximately 1.7 before entering the test channel. The channel was 2.54 cm in diameter, and the length between the anode and the cathode was 10 cm. The anode and cathode were used to apply an axial electric field along the arc heater chamber. The voltage gradient was measured by 20 circular probe electrodes, which were separated by boron nitride spacers along the channel. Garrison's experiment indicated that the electrical conductivity of potassium-seeded nitrogen plasma can be predicted with sufficient accuracy. He also conducted an analysis of the boundary layer correction, which showed that the effect of the current displacement thickness is minor and can be neglected.

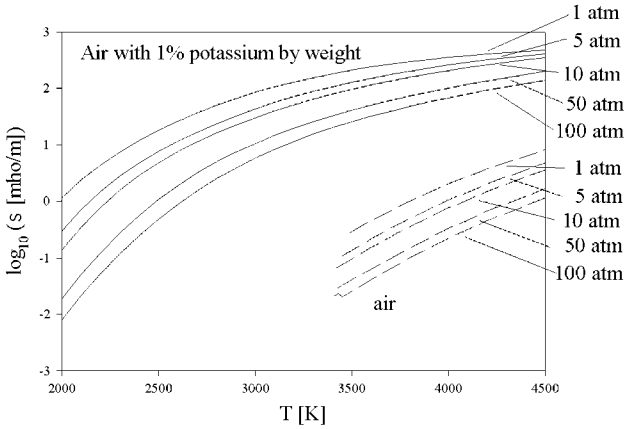

Figure 1. Theoretical conductivity of air, unseeded and seeded with 1% weight fraction of potassium.

A version of the NASA CEA code [15] that employs the Demetriades–Argyropoulos model was used in the present study to calculate the electrical conductivity at high pressures. These results for pressures from 1 to 100 atm and temperatures from 2000 to 4500 K are shown in figure 1 as dashed lines. The calculations for air are arbitrarily terminated below 3400 K because the conductivity level is insignificantly low. The electrical conductivity with 1% weight fraction of potassium carbonate as seed material was also calculated and is shown in the figure as solid lines. (A similar calculation was done for caesium, which achieves a slightly higher conductivity level than potassium for the same conditions.) As can be seen in the figures, electrical conductivity increases with temperature but decreases with pressure. Further, at low temperatures where conductivity is insignificant for the unseeded gas, the theory shows that the seeded gas achieves a dramatic increase of as much as 3 orders in magnitude increase in electrical conductivity. Alkali seeding has been suggested by various authors [5, 6, 16] as a means of increasing the electrical conductivity of high-temperature gases, within the context of hypersonic vehicle and ground test applications, due to the low ionization potential of alkali salts.

The theoretical results for both the unseeded and seeded gas indicate that there may be difficulties in achieving adequate ionization levels under high-pressure conditions. Nonetheless, the theoretical results need experimental verification. Such experiments are proposed to determine the conductivity of seeded gases so as to improve the understanding of weakly ionized gases at conditions of interest in propulsion and test facility development. In the following paragraphs, a conductivity channel and other hardware needed to perform the experiments are described. Some results are summarized together with a discussion of the discrepancy between experiment and theory.

3. Experimental apparatus

3.1. Shock tube

A high-performance, detonation-driven shock tube is used for the experiments to achieve the enthalpy and pressure conditions of interest. One of a number of different shock-tube configurations is shown schematically in figure 2 and is briefly

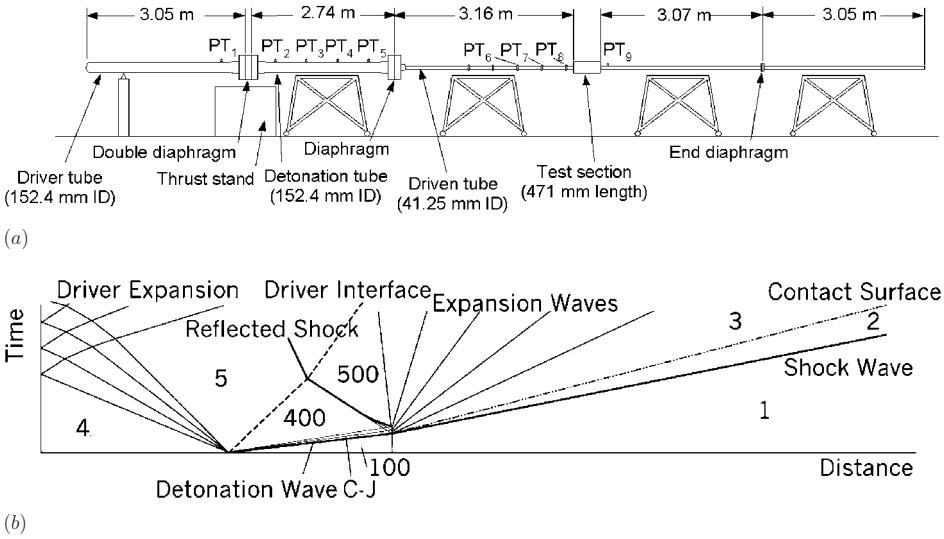

Figure 2. Shock-induced detonation-driven shock tube. (*a*) Schematic and (*b*) simplified wave diagram for specified geometry (thick line: shock or detonation wave, thin line: expansion wave, chain line: contact surface).

described; see [17] for more details. The shock tube consists of three major sections, namely, the driver, the detonation and the driven sections. The driver section (filled either with air or helium) has a bore of 152.4 mm and a length of 3.05 m while the detonation section (usually filled with stoichiometric oxyhydrogen), also with a bore of 152.4 mm, is 2.74 m long. These tube sections are rated for a pressure of 408 atm and they are separated by a double-diaphragm section. The diaphragms are made from 3.42 or 2.66 mm hot-rolled 1008 steel plates, scored to various depths in a cross pattern. The scored sides face downstream.

The detonation tube is attached to the driven tube via a flange which holds a 0.35 mm thick mylar diaphragm. The approximately 9.5 m long driven tube with a 40 mm bore produces a 14.5:1 area reduction. The pressure rating of the driven tube is 188 atm. The test section, comprising the electrical conductivity channel (to be described later), is located 3.16 m from the primary diaphragm location and has an overall length of 471 mm. Another section of the driven tube, that can be as long as 6.12 m depending on test conditions, is installed downstream of the test section to prevent wave reflections from the open end from interfering with the test flow. A 0.35 mm thick mylar diaphragm is inserted 3.07 m downstream of the test section to contain the initial driven tube gas.

The detonation tube has a port for filling and another for purging. Hydrogen and oxygen are injected through separate lines for safety. The detonation tube is evacuated through the hydrogen line to 0.02 atm. The hydrogen line is also used for venting the tube after a run or for purging the combustible mixture if there is an abort. Helium and purge air are injected through the oxygen line.

The filling and purging systems for the driver and driven tubes are relatively simple because they do not use reactive gases. Separate vacuum systems are used to evacuate these tubes to 0.02 atm. The driver tube is filled to the desired pressure with either air or helium. If there is an abort, the tube can be vented. Similarly, the driven tube is evacuated before being filled with dry air. The double-diaphragm chamber separating the driver and detonation tubes is filled with air at about half the pressure of the driver tube. A run is initiated by releasing the pressure in the double-diaphragm section. This causes the upstream diaphragm to rupture, which immediately causes the downstream diaphragm to also rupture. The high-pressure gas in the driver tube expanding into the detonation section propagates a shock wave which rapidly transitions into a detonation wave, as depicted in figure 2(*b*) which features an underdriven mode of operation [18]. The propagating detonation wave then impinges the thin downstream diaphragm to rupture it. The area reduction causes part of the wave to be reflected. This partial reflection traps high-pressure gas in a fashion similar to a reflected shock tunnel and serves to alleviate attenuation from the Taylor rarefaction, thereby prolonging the duration of uniform flow within the driven tube.

A shock wave propagates through the driven tube, followed by a contact surface and an unsteady expansion. As configured in figure 2, the test flow is region 2. The location of the conductivity channel and the length of tube attached downstream of it ensures an adequate slug of test gas.

The detonation driver instrumentation included five PCB (Depew, New York) model 111A22 piezoelectric pressure transducers PT_1–PT_5 and an MKS (Andover, Massachusetts) model 127A Baratron pressure transducer. The Baratron transducer has a maximum pressure range of 1.33 MPa and was used to set the mixture ratio during filling of the detonation driver. The PCB transducers are mounted in the driver tube with the sensing diaphragm flush with the inside wall. Each has a full-scale range of 68.9 MPa, rise time of 2 ms and a time constant of 1000 s. The Baratron transducer is used to provide an initial pressure reading for the dynamic PCB pressure transducers.

The driven tube instrumentation also includes four PCB transducers, namely, PT_6–PT_9. Two of these were PCB model 111A23 which has a full-scale pressure range of 34.4 MPa, rise time of 2 ms and a time constant of 500 s. These transducers are used primarily for shock speed measurements as they are upstream of the test area and separated by a precisely measured

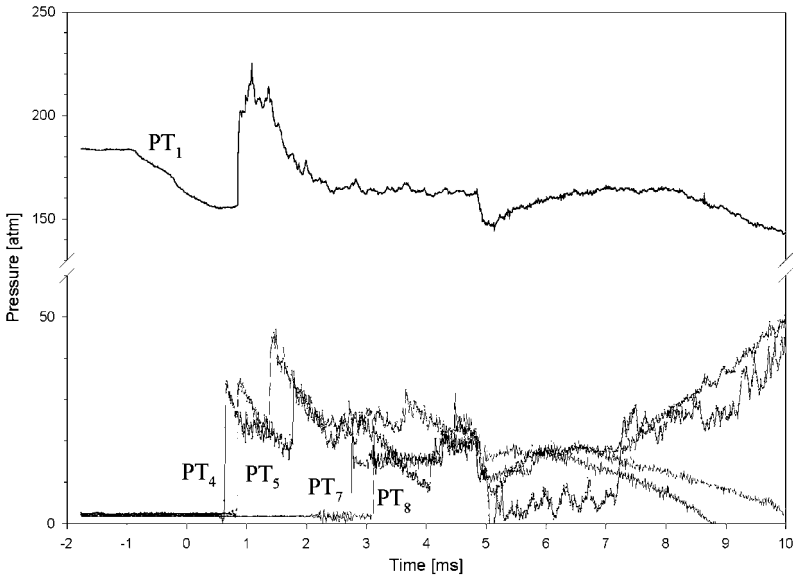

Figure 3. Sample pressure traces.

distance. The other two PCB transducers were either models 111A23 or 111A24, depending upon the conditions in the driven tube. The model 111A24 transducers have a full-scale range of 6.89 MPa, a response time of 2 ms and a time constant of 100 s. The initial pressure in the driven tube is also measured by a MKS model 127A Baratron pressure transducer. This transducer has a maximum pressure range of 133 kPa. This transducer provides an accurate measure of the initial driven tube pressure and also provides an initial pressure for the PCB transducers.

The pressure transducers are connected to a DSP Technology (Spectral Dynamics, San Jose, California) data acquisition system which has 48 channels capable of a 100 kHz sampling rate per channel, 12 bits of range, with each channel having its own amplifier and analogue-to-digital converter to allow for simultaneous sampling of all channels. The system has 512 kilosamples of total memory available to be shared between the channels being utilized. Eight channels are also available with a 1 MHz sampling rate, 12 bits of range and also with separate analogue-to-digital converters for each channel. Two megasamples of memory are available for these eight channels. The data acquisition system was controlled by a PC via an IEEE-488 interface. The data were then stored in the PC for later analysis.

The pressure transducers provide direct measurement of pressure ratios upon passage of the detonation or shock waves. Furthermore, time-of-flight measurements are used to calculate wave propagation speeds. Since the transducers are at a known distance apart, the shock or detonation velocity can be determined from the measured time interval between the observed pressure rise on adjacent pressure transducers. This provides an important indication of the properties of the detonation wave, primarily that the wave has indeed transitioned to a fully developed Chapman–Jouguet wave.

A sample of the pressure traces in the three major sections of the shock tube is shown in figure 3. These pressure traces can be interpreted with the aid of the wave diagram shown in figure 2(*b*). Transducer PT_1 detects the upstream

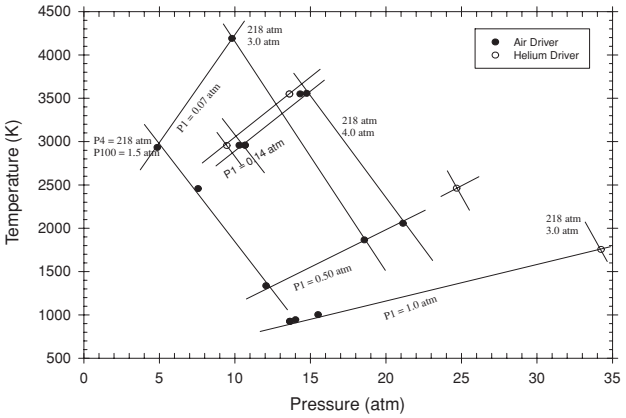

Figure 4. Shock-tube performance in terms of total pressure and total temperature in the driven tube.

propagating expansion wave when the diaphragms rupture at about −1 ms. The pressure spike at around 0.7 ms is due to the propagation of the reflected shock from the detonation tube. Subsequently, the pressure in the driver tube generally decreases as the gas vents through the detonation and driven sections. Transducers PT_4 and PT_5 record the detonation wave propagation in the detonation tube. A time-of-flight analysis indicates that a fully developed Chapman–Jouguet wave exists at those measurement stations [17]. The subsequent wave reflections due to the area reduction between the detonation and driven sections are also visible in these pressure traces. Due to this area constriction, the subsequent blowdown is, in fact, not immediately achieved. In fact, the pressure rises after 7 ms as the driver gas fills the detonation section. The shock wave that propagates into the driven section is clearly seen in the PT_7 and PT_8 traces. A useful test window of at least 1 ms is achieved. The subsequent blowdown in the driven section is clearly visible.

A composite performance map for the shock-induced detonation-driven shock tube is shown in figure 4. The

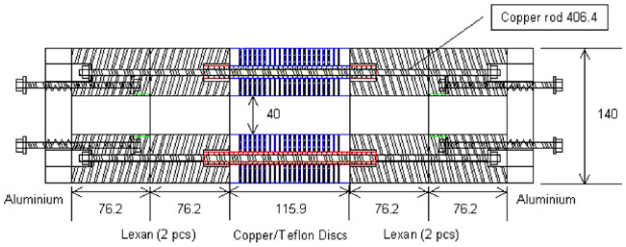

Figure 5. Sectional view of measurement channel (dimensions in mm).

peak shock Mach number obtained with the air driver is 10.71, resulting in a post-shock temperature and pressure of 4190 K and 9.8 atm, respectively. The highest post-shock pressure attained with the air driver is 21 atm, with a corresponding temperature of 2060 K. Use of helium in the upstream driver results in a considerable improvement in performance, as anticipated. There is a general increase in both temperature and pressure over that attainable with the air driver for comparable initial pressure and temperature conditions.

3.2. Measurement channel

The plasma electrical conductivity is measured in a channel connected to the end of the driven tube. The conductivity measurement channel consists of a pair of power electrodes and 20 probe electrodes separated by insulators in a design adapted from [10]. The total length of the measurement channel, including the power electrodes, the probe electrodes and the insulators, is 115.9 mm. The measurement channel is isolated from the shock tube on either side by 152.4 mm long lexan insulators. The entire apparatus is capped by 25 mm thick end flanges on either side. The electrodes and insulators are assembled together by clamping them with four threaded steel rods. These rods are sheathed by ceramic tubing to isolate them from the electrodes (figure 5).

The electrodes are made of oxygen-free copper which has an electrical resistivity of 1.69 $\mu\Omega$ cm at 300 K. The pair of power electrodes at each end of the channel provides an axial electrical field. Their inside and outside diameters are 40.03 mm and 139.7 mm, respectively, and their thickness is 9.53 mm. The dc excitation for this anode–cathode pair is provided by a capacitor bank which will be described below.

Other than the above-mentioned pair of power electrodes at the ends of the measurement channel, there are 20 probe electrodes for measuring the voltage drop along the channel. The probe electrodes have the same dimensions as the power electrodes except that they are only 3.18 mm thick. Teflon rings 1.59 mm thick are used to insulate the copper electrodes. Despite its low melting point, the teflon material is exposed to an extremely short heating pulse which allowed its use in the shock tube. However, experience shows that it is necessary to check the teflon rings for wear.

The conductivity channel is subjected to large pressures, both during the shock passage and later during the blow down of the detonation driver. A mishap caused some of the teflon and copper discs to be blown out. To prevent a further occurrence, an aluminium containment structure is used to reinforce the conductivity channel. Figure 6 is

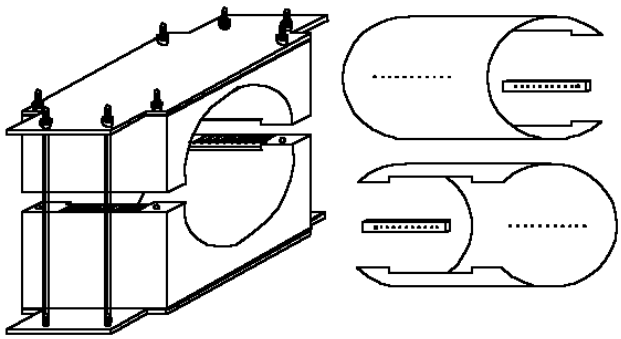

Figure 6. Pressure containment structure for conductivity channel.

a schematic of this containment covering the conductivity measurement channel. The conductivity channel is encased in two layers of teflon (right side of the figure) prior to insertion into the containment structure to prevent shorting of the applied voltage. The electrical wiring is channelled through holes in two teflon blocks and the two teflon wraps. The containment structure extends beyond the conductivity channel on both upstream and downstream ends to also encase the lexan insulator rings. The upper and lower halves of the containment structure are then securely held by threaded screws bolted at each end to top and bottom caps (left side of the figure). In this way, the internal pressures are transferred to eight high-strength bolts.

3.3. Power supply

To design the components of the excitation circuit, the gas electrical conductivity must be known. Ohm's law indicates that the current is a function of the applied external electric field and the electrical conductivity, that is,

$$E = \frac{I}{\sigma A}. \tag{3}$$

This equation can be rearranged to yield

$$\sigma = \frac{I}{AE} = \frac{IL}{AV}, \tag{4}$$

where I is the total input current, A is the effective area of current conduction, L is the length of the measurement channel and V is the voltage drop along the channel.

For a measurement channel with fixed bore and length, and a given input current, the applied electric field and current flow are functions of electrical conductivity. An example of such a calculation for air at 3000 K, with a 1% caesium carbonate seeding, is displayed in figure 7 for the present configuration. The calculations made use of the modified CEA code. Figure 7 shows the current and voltage as a function of gas pressure. Not displayed are results showing the effect of pressure and seed concentration. The figure shows that as the current density increases, the electrical conductivity also increases. The increase in conductivity is due to Joule heating of the gas and also due to the fact that the electron temperature is raised higher than the gas temperature, although the elevation of electron temperature is generally small for gaseous molecular species. From (4), given the dimensions of the measurement channel, A and L, the values of conductivity obtained from the calculations enable the current and voltage

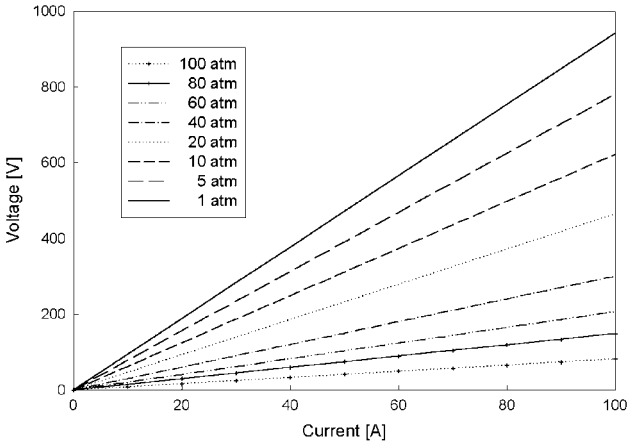

Figure 7. Power electrode current and voltage requirements for air with 1% weight fraction of caesium at 3000 K.

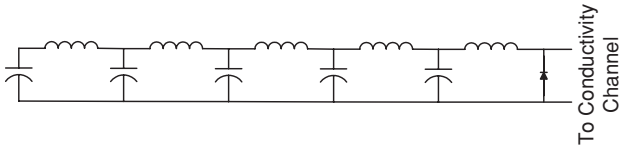

Figure 8. Example of a pulse-forming network.

Table 1. Power supply design parameters.

T (K)	p (atm)	σ (℧ m^{-1})	Z (Ω)	C_t (μF)	L_t (mH)	V (V)
4000	1	423	0.218	2300	0.109	22
4000	100	95.3	0.966	517	0.483	97
3000	1	132	0.698	716	0.349	70
3000	100	12.7	7.25	69.0	3.63	725
2500	1	37.6	2.45	204	1.22	245
2500	100	1.62	56.8	8.80	28.4	5680
2500	25	6.23	14.8	33.8	7.40	1480
2500	50	3.36	27.4	18.2	13.7	2750
2500	75	2.22	41.5	12.0	20.8	4150

to be specified. Thus, the power supply can be sized. It is appreciated that the conductivity so calculated is meant to provide a guide in the design. In the experimental programme, the reverse procedure is undertaken, in which the current and voltage are measured and the conductivity is obtained from (4). The experimental values of conductivity are then compared with the computed values to validate the theoretical model.

The excitation for the power electrodes comes from a capacitor–inductor bank. The capacitor–inductor bank is designed according to methods outlined in [19] to discharge with a steady current and voltage in about 1 ms, which exceeds the expected test duration. Thus, the relationship between discharge time t_d, the load impedance Z and the total supply capacitance C_t or total supply inductance L_t is

$$t_d/2 = ZC_t = L_t/Z. \tag{5}$$

A network of five capacitors and inductors, shown schematically in figure 8, was used, each being one-fifth of the value calculated from (5). A sample of the calculated values is shown in table 1. The load voltages shown in the final column are for a current of 100 A. Lower current levels would require lower voltages. The table shows that different combinations of capacitors and inductors are needed to deliver the desired

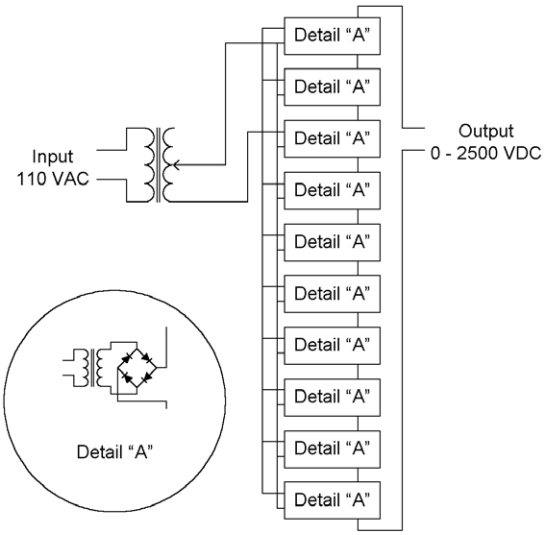

Figure 9. Charging circuit.

potential. Off-the-shelf capacitors of 40, 50 and 55 μF, rated to 440 V, were used in different series and parallel combinations. The inductors were formed by wrapping copper wire around a cylindrical iron core. The inductance was calculated by

$$L = \mu AN^2/l \tag{6}$$

where μ is the permeability of iron, l is the core length, A is the cross-sectional area of the core and N is the number of turns. The calculation assumes that the magnetic field lines are contained in the core. A cylindrical core does not completely contain the magnetic field lines over their entire length. Therefore, the value of the permeability must be corrected to account for this. Fine adjustment of the inductance value is obtained with an inductance meter.

The pulse-forming network was designed for a maximum potential of 8 kV. The inductors reduce both the rate of discharge of the capacitors to the time required and the amount of overshoot of the current from the steady-state value. The current tends to oscillate at the end of the discharge. Therefore, a diode is connected across the output leads to eliminate this and reduce the voltage seen by the capacitors, resulting in increased capacitor life. The capacitor bank open circuit voltage was applied to the conductivity channel prior to firing the shock tube. The seeded air plasma following the incident shock wave served as the switch to initiate current flow.

The capacitor bank is charged between each run. During this charging process, it is isolated from the measurement channel. A charging unit was designed to charge the capacitor assemblies up to 2.5 kV (see figure 9). For voltages above this, the capacitors were separated by switches to allow them to be charged as assemblies and then reconnected in the proper configuration for operation. This allowed the charging unit to be smaller, less expensive and constructed with off-the-shelf components.

3.4. Seeding material and seed injection system

An apparatus was designed to inject seed materials upstream of the electrical conductivity channel (figure 10). The weight fraction of seed materials, either potassium or caesium, was

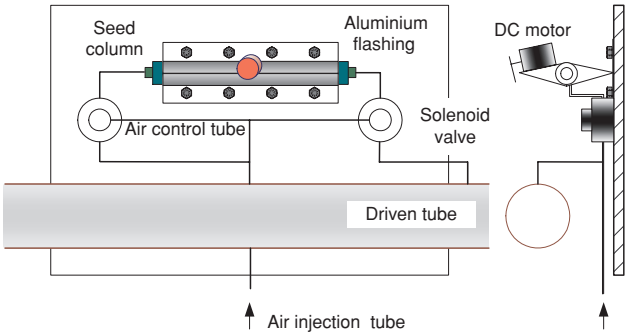

Figure 10. Seed injection apparatus.

calculated based on the anticipated test conditions. An Acculab (model V-1mg) scale with a sensitivity of 1 mg and capacity of 120 g was used to measure the desired amount of seed material.

An off-the-shelf chromatography column, 10 cm long and 1.1 cm bore, was used to hold the seed material prior to injection. This column is rated to 41 atm and it was sealed by two endpieces containing ◯ rings. PTFE barb-type connectors were used to connect the PTFE tubing to this column assembly. The PTFE tubing has a 0.158 cm bore and 0.3175 cm outside diameter and is rated for 34 atm.

Two 12 VDC solenoid valves are used to control the inlet and outlet air flow through the seed injection column assembly. The solenoid valves supply actuation air at a pressure of 2.7 atm. During the injection operation, the outlet valve is opened first to allow the seed to be sucked into the evacuated driven tube. Then the inlet valve is opened for only a few seconds to provide the high pressure (maximum 2.7 atm) needed to force the remaining seed material into the driven tube. With the help of a vibrator, it is only necessary to open the inlet valve for about 10 s to inject the entire mass of seed material into the driven tube. The pressure rise in the driven tube due to the injection process is less than 0.07 atm. The diaphragm chamber was then vented to initiate the run. The time between the end of the seeding process and the actual burst of the diaphragms is about 5 min.

The vibrator device is made of two pieces of aluminium flashing. One end of each of these two strips of flashing is mounted to the board supporting the injection system. The other ends of these strips are riveted together to form a cantilever spring. The column assembly is clamped in between these aluminium strips. A 9 VDC motor is set on the upper side of this assembly with an eccentric rubber disc attached to the shaft. When the motor was activated by a 9 V battery, the end of the cantilever spring vibrated up and down which helps to suspend the particles in the column, so that they are more easily entrained into the injection air stream.

A retractable nozzle for dispersing the seed into the driven tube, with two orifices pointed along the longitudinal axis of the driven tube, is attached to the outlet of the injection system. The nozzle is retracted by a coil spring when the injection system is not operating, and is pushed into the driven tube by the applied inlet air pressure. The parallel open ends are designed to spread the seed material evenly in the driven tube.

Bench testing of the system shows that either a higher inlet air pressure or a longer injection period gave a more uniform seed material distribution in the driven tube. The higher inlet pressure serves to push the seed material further away from the injection point. The longer injection time provides more air to suspend more of the seed material inside the driven tube.

There are, however, two drawbacks to this approach. First, precisely setting the initial pressure in the driven tube is a critical factor for determining the test conditions. Allowing the driven tube pressure to be changed by the seed injection causes the test conditions to vary from test to test. Secondly, the increased injection time agitates the seed material inside the driven tube. This may also have the undesirable effect of causing the seed material to be pushed to the far ends of the driven tube or downstream of the conductivity channel. Both of these effects detract from the ability to obtain repeatable results from test to test.

3.5. Data reduction and uncertainty

The uncertainty in the initial pressure in the driven tube p_1 is $\pm 16\%$ partly due to the aforementioned need to inject the seed material with high-pressure air. The high uncertainty of initial pressure is primarily due to the inability to measure the initial pressure with the Baratron pressure transducer just prior to rupturing the diaphragm. The Baratron pressure transducer needed to be isolated prior to firing the shock tube to prevent it from being damaged from over-pressurization. Unfortunately small leaks in the measurement channel allowed the pressure to rise to an unknown amount between the isolation of the transducer and rupture of the diaphragms to initiate the flow. This factor will not affect the accuracy of the shock speed calculation, but will cause problems in setting the precise pressure ratio required to achieve a desired shock speed. However, the temperature uncertainty is $\pm 1\%$. An inverse calculation using the measured value of p_2 and the measured shock speed was used to obtain p_1. This procedure yielded an accurate determination of test conditions for each run, but precluded good repeatability. The shock speed u_s is calculated from time-of-flight measurements of shock passage past the two transducers on each side of the conductivity channel. The uncertainties in the shock speed u_s, and the post-shock pressure and temperature p_2 and T_2, are $\pm 1.4, \pm 5.4$ and $\pm 5.5\%$, respectively.

The seed mass is measured to an accuracy of $\pm 1.3\%$, which is also the uncertainty in the seed mass fraction. The low value of the uncertainty in the seed fraction is based on the assumptions of uniform entrainment of seed in the air, which means there is no settling to the bottom of the driven tube. Also the seed mass is calculated from the initial driven tube conditions determined from p_1, T_1 and the density before the driven tube is evacuated to the desired pressure. Because these initial conditions p_1, T_1 of the driven tube can be precisely determined, they have a negligible effect on the uncertainty of the seed mass fraction. Therefore, the dominant parameter involved in this analysis is the scale accuracy, which is used to measure the required amount of the seed material. The seed mass is also assumed to remain constant during the evacuation of the driven tube. But subsequent analysis indicates that the seed material is not distributed uniformly along the driven tube. The incomplete ionization and vaporization of the seed material also reduces the amount of the seed material in the test gas.

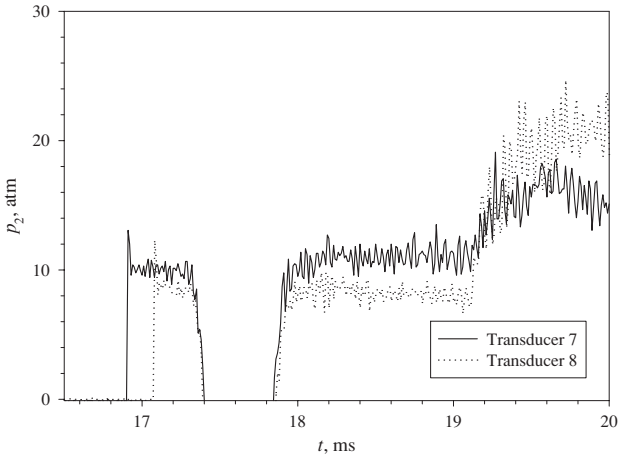

Figure 11. Example of test data: pressure. Transducers 7 and 8 are 75.88 cm and 20.16 cm from the upstream face of the conductivity channel.

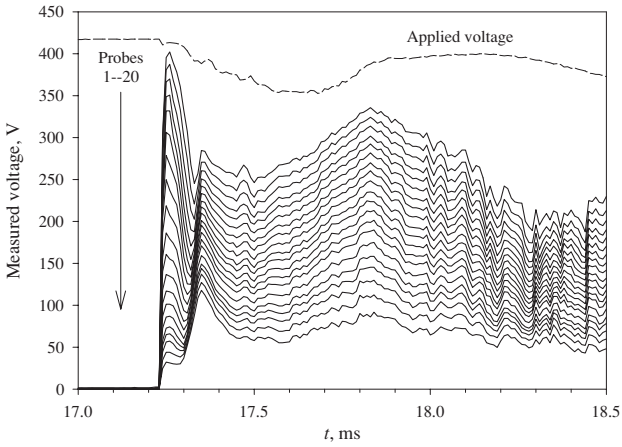

Figure 12. Example of test data: voltage.

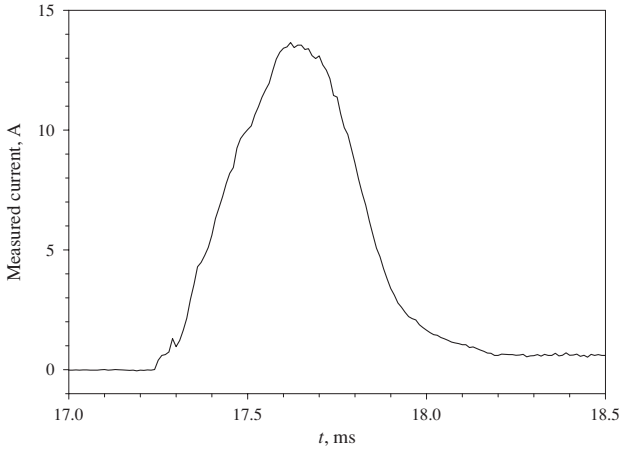

Figure 13. Example of test data: current.

The current and voltage are both measured to an accuracy of $\pm 1\%$. Finally, the average conductivity is accurate to $\pm 4.6\%$. The uncertainty in average conductivity is principally due to the uncertainty in two major measurements: the magnitude of the electrode voltage drop and the length of the end effect region. An accurate measurement of voltage drop between the powered electrode and the measurement probe is difficult to obtain, and the length over which the voltage is measured in the conductivity channel is not precisely known.

4. Sample results and discussion

All the runs exhibited similar features and the key features of an example run are now discussed. The nominal conditions for this example are $M_s = 7.76$, $T_2 = 3010$ K, $p_2 = 8.5$ atm, $V_A = 400$ V and $S = 1\%$. The pressures just upstream of the conductivity channel are shown in figure 11. The shock speed, together with initial conditions, enabled the post-shock pressure p_2 and temperature T_2 to be calculated using CEC [15]. Previous calibrations indicated agreement between the measured and calculated values for p_2 to within 5%.

Figure 11 shows unusual behaviour at $t \approx 17.3$ ms during which the measured pressure vanished. This is thought to be due to interference induced in the piezoresistive pressure transducers from the current flow in the channel. This phenomenon was not observed at low currents. The abrupt change in transducer output at $t \approx 17.3$ ms coincides with the start of current flow in the channel. The transducer readings returned to a fairly steady level at $t \approx 18.1$ ms. This coincides with the current decaying to near zero.

Figure 12 shows the voltage traces. The top curve is the applied voltage across the powered electrodes. The probe electrodes did not sense any voltage until passage of the ionized flow following the incident shock. The electrode voltages reached a maximum value in about 20 μs and then dropped due to current flowing from the capacitor bank. The estimated test time for this case was about 185 μs. The voltages then rose to a second peak as the applied voltage from the capacitor bank increased.

The current peaked at about 17.6 ms, which coincides with the minimum in the applied voltage. This is shown in figure 13. The peak current occurred about 210 μs *after* the estimated time for passage of the contact surface through the conductivity channel. The rate of current rise was slower than the designed rate and this was initially thought to be due to an impedance mismatch between the power supply and the plasma load. However, a simulation of the transient characteristics of the power supply indicates that the current rise time should be 10–20 μs. The estimated rise time calculated during the design of the power supply was 80–100 μs. The analysis suggests that a more probable cause of the slow rise time is an actual variation in plasma resistance with time. The plasma resistance variation could be due to the time required for vaporization, dissociation and ionization of the seed. A second possibility would be the non-uniform seed distribution in the driven tube. The residual seed produced measurable conductivity in the detonation products following the test flow, as indicated in the figures.

The voltage data were reduced to axial voltage gradients at the time of peak current and at the passage of the contact surface and shown in figure 14. The end effects between the power electrodes and the adjacent probe electrodes, in the form of higher voltage gradients, are clearly seen. The voltage across the 20 probe electrodes is shown in figure 15. The voltage difference reached a peak of about 250 V and then dropped to about 135 V as the current rose to its peak value

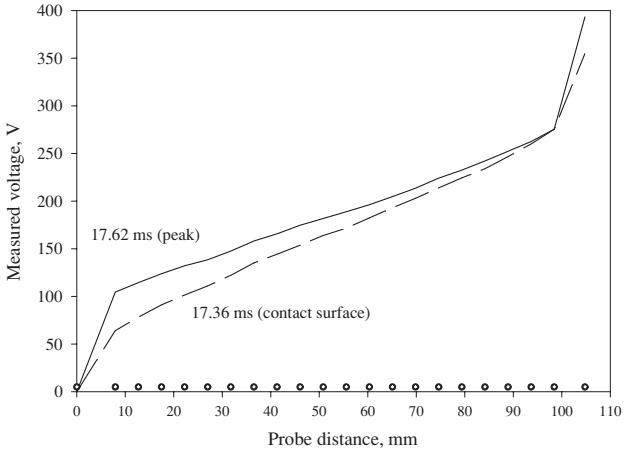

Figure 14. Example of test data: voltage gradient. Circles represent the midline of the electrodes.

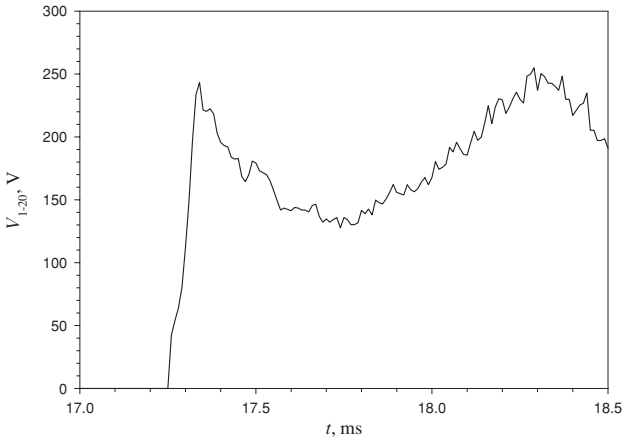

Figure 15. Example of test data: voltage difference across the 20 probe electrodes.

at $t \approx 17.6$ ms. This trend is in general agreement with the Nottingham model [20] which gives the following relation for the electrode voltage drop:

$$\Delta V = C_1 + C_2/I^n. \tag{7}$$

The voltage difference then rose, probably due to an increase in boundary layer thickness as the incident shock wave moved downstream.

The average conductivity between the first and last probe electrodes can be expressed as

$$\sigma^*(t) = \frac{I(t)/A}{V_{1-20}(t)/x_{1-20}} \tag{8}$$

where the arguments indicate the transient nature of the flow. The voltage drops between the power electrodes and the adjacent probe electrodes were neglected because they included extraneous effects such as surface work functions, voltage drops across the boundary layers and curvature of current filament lines in the powered electrode region. However, the probe electrodes did not suffer from such effects and the voltage gradient exhibited linear behaviour, as can be seen in figure 14. The average conductivity, displayed in figure 8, closely followed the measured current variation.

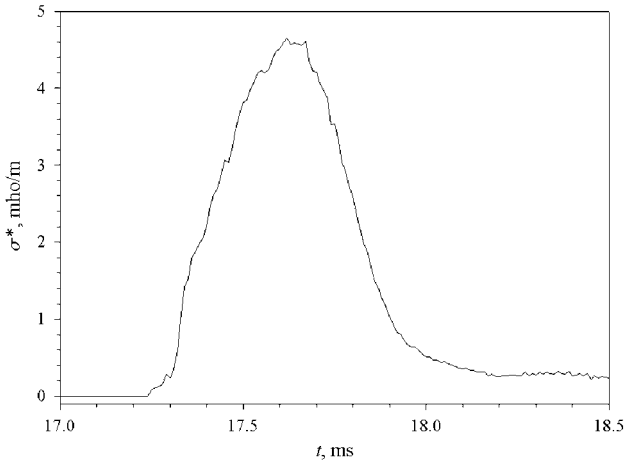

Figure 16. Example of test data: average conductivity.

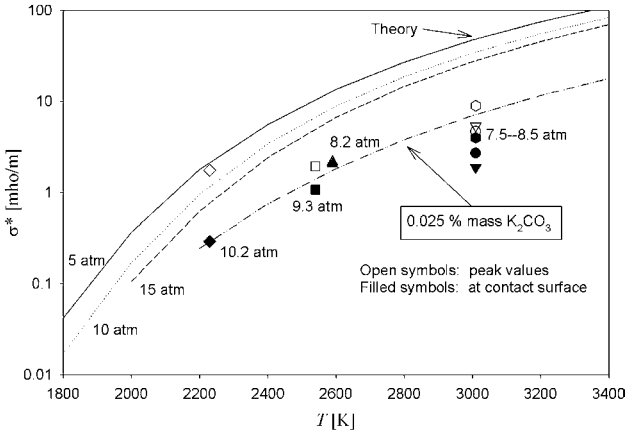

Figure 17. Experimental and theoretical conductivities of air at 10 atm with 1% mass fraction of potassium carbonate.

4.1. Comparison with theoretical models

The measured average conductivity for air at 10 atm is shown in figure 16. The data were taken at the peak conductivity and at the arrival of the contact surface at pressures varying from 7.5 to 10.2 atm, as indicated in the figure. The figure also shows values at 5, 10 and 15 atm obtained using the theory outlined in [10]. In general, the measured conductivities are lower than the theoretical values. Figure 17 shows that measured conductivities behind the contact surface are higher than those in front of the contact surface.

Possible reasons for the discrepancy between experiment and theory include boundary layer blockage, Joule heating and poor seed entrainment by the flow. The effect of the boundary layer was checked by a previously developed, time-accurate Navier–Stokes code, from which the boundary layer thickness δ and the axial electrical displacement thickness

$$\frac{\delta_j^*}{R} = \int_0^{\delta/R} \left(1 - \frac{J_x}{J}\right)\left(1 - \frac{r}{R}\right) \mathrm{d}\left(\frac{r}{R}\right) \tag{9}$$

were obtained [22]. The boundary layer thickness is typically about 0.12 mm, which is small compared to the radius of the channel, while the current displacement thickness is typically about 1.2 mm. The effective core area for the current

$$A_c* = \pi(R - \delta_j^*) \tag{10}$$

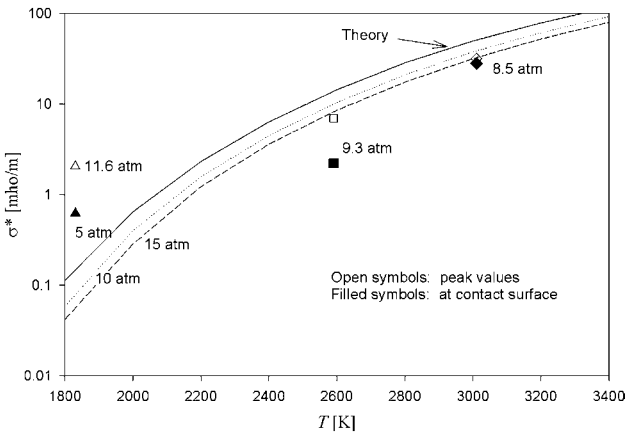

Figure 18. Experimental and theoretical conductivities of nitrogen at 10 atm with 1% mass fraction of potassium.

is therefore about 11.14 cm^2 compared to the geometric cross-sectional area of 12.59 cm^2. The ratio of the core conductivity and the measured conductivity is $\sigma_c/\sigma = A/A_c^*$. Thus, the boundary layer blockage reduced the core area for current flow. Accounting for the blockage raised the experimental conductivity by about 12%, but this was not sufficient at the higher temperatures to account for the discrepancy between theory and experiment.

Joule heating was found to raise the temperature from the front to the rear of the conductivity channel by about 2 K. Its effect on conductivity was, therefore, negligible.

Finally, the poor convection of seed appeared to be the most plausible reason for the low experimental values. One indication of this is the presence of current after the slug of test gas has passed. The large particle size resulted in settlement to the bottom of the driven tube between seed injection and run. Moreover, the large particle size also required a long time, of the order of a few ms, for dissociation and ionization to complete. Calculations of electrical conductivity at reduced seed mass fractions were made, and the results for a seed mass fraction of 0.025% are compared with experimental data in figure 17. Note that the general trend of conductivity with temperature is well correlated with the experimental data. Thus, we conclude that the primary reason for the discrepancy is due to a combination of settlement of seed particles from the gas during the time between seed injection and firing the shock tube and insufficient time for complete vaporization of the remaining seed particles.

A comparison between experimental and theoretical conductivities for a seeded nitrogen plasma at 10 atm is presented in figure 18 for temperatures from 1830 through 3010 K. The flow Mach numbers ranged from 5.49 for the highest temperature through 7.76 for the lowest temperature. Experimental conductivities for seeded nitrogen are higher than for seeded air. The measured conductivity ranged from 75–85% of theoretical values at higher temperatures to 2–3 times theoretical values at lower temperatures. Thus, the phenomenon of electron attachment by positive oxygen ions postulated by Simmons *et al* [21] appears to have some degree of validity.

5. Conclusions

The basic electronic conductivity measurement device first proposed by Garrison [10] was used in a shock-tube environment. In general, agreement between experimental and theoretical conductivities was fair at nominal pressures of 10 atm for the small amount of seed used. The results of the conductivity measurements with a seeded nitrogen plasma appear to give some support to the theory of electron attachment by the positive oxygen ions in a seeded air plasma. Measured conductivities for the nitrogen plasma were on the order of 2–3 times larger than comparable measurements for the air plasma, whereas the CEC with the Demetriades–Argyropoulas conductivity model produced comparable results for the two plasmas. The experiments showed that the conductivity channel performed well despite problems with seeding. However, the data are one to two orders of magnitude lower than theoretical results. The primary reason for the discrepancy is thought to be due to a combination of settlement of seed particles from the gas during the time between seed injection and firing the shock tube and insufficient time for complete vaporization of the remaining seed particles. However, we still feel that the basic approach is a viable method for measurement of electrical conductivity of seeded plasmas, and furthermore, gives an assessment of the effectiveness of the seeding system.

Acknowledgments

We gratefully acknowledge MSE, Inc., Butte, Montana for funding the development of the conductivity channel and the detonation-driven shock tube. We are also grateful for numerous discussions with Dr Ying-Ming Lee (presently with RSR Inc., Loomis, California) and Mr Gloyd Simmons of MSE, Inc. Finally, we acknowledge the assistance of Messrs Chul-Han Kim, Jimmie Holland and Scott Stuessy with the experiments, as well as useful discussions with Dr Ramakanth Munipalli.

References

[1] Munipalli R, Anderson D A and Wilson D R 2000 CFD evaluation of seeded and unseeded air MHD accelerators *AIAA Paper* 2000-0215

[2] Vatazhin A B and Kopchenov V I 2000 Problem of hypersonic flow deceleration by magnetic field *AIAA Progress in Aeronautics and Astronautics: Scramjet Propulsion* vol 189 ed E T Curran and S N B Murthy (Reston, VA: AIAA) chapter 14

[3] Brichkin D I, Kuranov A L and Sheikin E G 1998 MHD-technology for scramjet control *AIAA Paper* 98-1642

[4] Litchford R J, Thompson B R and Lineberry J T 2000 Pulse detonation magnetohydrodynamic power *J. Propulsion Power* **16** 251-62

[5] Cambier J-L 1998 MHD power generation from a pulse detonation engine *AIAA Paper* 98-3876

[6] Nelson G L and Simmons G A 1995 Augmentation of hypersonic propulsion test facilities using MHD *AIAA Paper* 95-1937

[7] Lin S C, Resler E L and Kantrowitz A 1955 Electrical conductivity of highly ionised argon produced by shock waves *J. Appl. Phys.* **26** 95–109

[8] Spitzer L and Harm R 1963 Transport phenomena in a completely ionised gas *Phys. Rev.* **89** 977

[9] Vincenti W G and Kruger C H 1977 *Introduction to Physical Gas Dynamics* (Huntington, NY: Krieger)
[10] Garrison G W 1968 Electrical conductivity of a seeded nitrogen plasma *AIAA J.* **6** 1264–70
[11] Allis W P 1956 *Handbuck der Physik* vol 21 (Berlin: Springer) p 95
[12] Frost L S 1961 Conductivity of seeded atmospheric plasmas *J. Appl. Sci.* **32** 1012
[13] Demetriades S T and Argyropoulos G S 1966 Ohm's law in multicomponent non-isothermal plasmas with temperature and pressure gradients *Phys. Fluids* **8** 2136–49
[14] Frohn A and De Boer P C T 1969 Measurement of ionization relaxation times in shock tubes *Phys. Fluids Suppl.* I I-54–7
[15] Gordon S and McBride B J 1994 Computer program for calculation of complex chemical equilibrium compositions and applications: I. Analysis *NASA RP-1311* http://www.grc.nasa.gov/WWW/CEAWeb/RP-1311.htm
[16] Kuranov A L, Chaika M and Ionikh Y 2001 Examination of a possibility of non-conventional use of alkaline admixture for ionization of atmospheric gasses *AIAA Paper* 2001-2952
[17] Lu F K and Wilson D R 2003 Detonation driver for enhancing shock tube performance *Shock Waves* **12** 457–68
[18] Lu F K, Wilson D R, Bakos R J and Erdos J I 2000 Recent advances in detonation techniques for high-enthalpy facilities *AIAA J.* **38** 1676–84
[19] Adler R J 1989 *Pulse Power Formulary* (Albuquerque, NM: North Star Research Corporation)
[20] Nottingham W B 1923 A new equation for the static characteristic of the normal electric arc *Trans. AIEE* 302–10
[21] Simmons G A, Nelson G L and Ossello C A 1998 Electron attachment in seeded air for hypervelocity MHD accelerator propulsion wind tunnel applications *AIAA Paper* 98-3133
[22] Munipalli R, Kim H, Anderson D A and Wilson D R 1997 Computation of unsteady nonequilibrium propulsive flowfields *AIAA Paper* 97-3164